A Better Dipole

Eugene d'Eon
Nov 14, 2012
(corrected Table 2 Dec 4, 2012)

Abstract

We present a dipole BSSRDF with modified diffusion asymptotics, improved exitance calculations and consistent boundary conditions. This BSSRDF improves significantly upon the classical dipole model, requires negligible extra evaluation cost and is very easy to adapt in new and existing subsurface scattering algorithms. While not as accurate as a diffusion model using an extended source, such as the recent quantized diffusion method, this dipole model is far easier to implement and is of potential interest in some rendering and measurement applications. We include a comprehensive quantitative comparison between the classical dipole and the "better" dipole as well as quantized diffusion and benchmark Monte Carlo results for reference.

Keywords: BSSRDF, dipole, translucent materials, modified diffusion

η	*relative index of refraction*
ρ	*number density of particles* [m^{-3}]
σ_a	*absorption cross-section* [m^2]
σ_s	*scattering cross-section* [m^2]
$\mu_a = \sum_k \rho_k \sigma_{ak}$	*absorption coefficient* [m^{-1}]
$\mu_s = \sum_k \rho_k \sigma_{sk}$	*scattering coefficient* [m^{-1}]
$\mu_s' = (1-g)\mu_s$	*reduced scattering coefficient* [m^{-1}]
$\mu_t = \mu_s + \mu_a$	*extinction coefficient* [m^{-1}]
$\mu_t' = \mu_s' + \mu_a$	*transport coefficient* [m^{-1}]
$\alpha = \mu_s/\mu_t$	*single-scattering albedo*
$\alpha' = \mu_s'/\mu_t'$	*reduced single-scattering albedo*
g	*mean scattering cosine*
D	*diffusion coefficient* [m]
A	*reflection parameter*
$L(\vec{x}, \vec{\omega})$	*radiance* [$\mathrm{W\,m^{-2}\,sr^{-1}}$]
$L_i(\vec{x}, \vec{\omega})$	*incident radiance* [$\mathrm{W\,m^{-2}\,sr^{-1}}$]

Table 1: *Nomenclature*

1 Intro

The utility of physically-based reflectance models for generating realistic computer generated images has been well demonstrated and shows no sign of decline. Given the broad range of applications, a wide array of reflectance models of varying accuracy continue to see use. The tradeoffs between simplicity, computational cost, ease of implementation and accuracy are subjective and vary highly with the problem being solved, so having many well-evaluated options will likely only extend the utility of physically-based reflectance models as a whole. This note presents a broad evaluation of two previous reflectance models for thick translucent materials and introduces a new model—not the most accurate—but more accurate than a previous model of similar complexity.

Accurately simulating the transport of light within translucent materials is challenging. The *bidirectional scattering-surface reflectance-distribution function* (BSSRDF) describing the scattering and bleeding of light through geometry resists exact solution, even for the most basic cases such as flat dielectric materials with a smooth boundary and a simple isotropic scattering process below the surface. However, some useful approximations have been found in this area based on diffusion theory.

We recently introduced a new diffusion-based BSSRDF for rendering images of homogeneous (or layered) translucent materials [D'Eon and Irving 2011]. In this previous work we pieced together a number alterations/additions to now "classical" diffusion methods. The goal was to extend the accuracy of the dipole and multipole approximations (the method of images) to the widest possible range of materials (and layerings of materials) relative to an error metric suitable for graphics. The evaluation of each independent alteration to classical diffusion methods introduced in [D'Eon and Irving 2011] was rather limited due to space limitations. It was mentioned that many of these individual alterations could improve upon previous methods, but this was not thoroughly demonstrated. The purpose of this note is to fill this gap.

Here we consider the BSSRDF of d'Eon and Irving [2011] but *without the extended-source term*. The benefit of doing so is to extend the reach of improved diffusion asymptotics and Fresnel-consistent boundary conditions in graphics (and potentially in other fields where the classical dipole expression repeatedly appears). The resulting model remains a dipole, which is simple to write down and evaluate (see Table 2) and avoids the complexity of the quantization of diffusion Green's functions into discrete Gaussian sums. Modification of any existing implementation of [Jensen and Buhler 2002] to use this new dipole should be trivial (whilst switching to a quantized diffusion BSSRDF is not). The evaluation below should make clear the potential gain in accuracy in doing so. The caveats are that this new dipole still lacks the high-frequency components of an extended-source BSSRDF, important for skin rendering. The analogous "better multipole" would see a similar improvement in accuracy (not demonstrated here) but would not be applicable to materials thinner than several mean free paths without the extended source term of [D'Eon and Irving 2011]. For the application of skin reflectance one could certainly attempt to mimic the missing high-frequency content of a dipole BSSRDF with an appropriate (and likely non-physical) multilayer multipole model, but the complexity tradeoff is then irrelevant, making quantized diffusion a more attractive, versatile solution.

This is in no way an endorsement for not using an extended source model. In fact, the results below help further demonstrate the improved accuracy to be gained by taking the effort to implement a BSSRDF like quantized diffusion. However, given the simplicity of the better dipole and the non trivial effort required to implement a quantized diffusion BSSRDF (and the additional optimizations required to achieve a computational performance similar to either dipole model), the current presentation seems relevant. Finally, given the broad scope of evaluation and the use of benchmark open source Monte Carlo code, we hope this note will also serve as a reference benchmark for any of the three analytic models we compare below.

2 Improving upon the classical dipole

To render translucent materials using a BSSRDF S, exitant radiance at a surface location $\vec{x}_o$ in direction $\vec{\omega}_o$ is computed by integrating

the incident radiance $L_i(x_i, \vec{\omega}_i)$ with S:

$$L_o(x_o, \vec{\omega}_o) = \int_A \int_{2\pi} S(x_i, \vec{\omega}_i; x_o, \vec{\omega}_o) L_i(x_i, \vec{\omega}_i)(\vec{n} \cdot \vec{\omega}_i)\, d\omega_i\, dA(x_i).$$

Since Grosjean [1958] it has been shown useful to separate light (or neutrons) into reduced-intensity, single-scattering, and multiple-scattering components, each treated separately,

$$S = S^{(0)} + S^{(1)} + S_d.$$

Here we only consider thick semi-infinite materials, so reduced-intensity transmission $S^{(0)}$ is irrelevant. Single scattering $S^{(1)}$ can be computed using previous methods such as the technique described in [Jensen et al. 2001]. The dipole model makes it appearance by assuming that multiple scattering can be described using a diffusion method of images solution to a 2D searchlight problem. If one assumes that light arrives normal to the surface and computes only the net flux leaving the surface at any distance r from the point of illumination then the problem being solved is much easier. If we also suppose that given the total flux leaving the surface at some location we can approximate its angular shape to be Lambertian (or Lambertian modulated by outgoing Fresnel shaping), then the full 8D BSSRDF can be replaced with a much simpler form [Jensen et al. 2001]:

$$S_d\,(x_i, \vec{\omega}_i; x_o, \vec{\omega}_o) = \frac{1}{\pi} F_t(x_i, \vec{\omega}_i) R(||x_i - x_o||_2) \frac{F_t(x_o, \vec{\omega}_o)}{1 - 2C_1(\frac{1}{\eta})}, \quad (1)$$

where $R(r)$ is a radially-symmetric *diffusion profile* $R(r)$ computed or measured using various methods and F_t is a Fresnel transmittance function. Equation 1 differs only slightly from the original seminal introduction by Jensen et al. [2001]—we have included the missing normalization constant described in [D'Eon and Irving 2011] (C_1 is given below). Occasionally the Fresnel terms F_t in Equation 1 are neglected to use Lambertian exitance shaping, or can also be replaced by integrals of rough BRDFs to handle rough surface boundaries, as proposed by Donner and Jensen [2005] (where an analogous normalization term is also missing). Our main focus here, however, is on the choice of $R(r)$. The visual character of light bleeding within the object and into shadow boundaries (as well as the overall color of a material) is based primary upon the choice of $R(r)$.

We compare three different analytic diffusion profiles $R(r)$,

- The classical dipole [Farrell et al. 1992; Jensen et al. 2001]
- A new better dipole model (defined below)
- Quantized Diffuion [D'Eon and Irving 2011].

The equations for the classical dipole and the new better dipole are compared in Table 2 where the moments C_1 and C_2 of the Fresnel function are given separately in Equation 2 (repeating the approximations given in [D'Eon and Irving 2011]). Both of these dipole models are compared to the quantized diffusion BSSRDF of d'Eon and Irving [2011] and to Monte Carlo simulation, neither of which are described here. The better dipole is derived by modifying the classical dipole to use the diffusion asymptotics of Grosjean [1956], the asymptotically consistent boundary conditions of Pomraning and Ganapol [1995], and the diffusion-consistent exitance calculation of Kienle and Patterson [1997]. The physical reasoning for adopting these alterations can be found in the mentioned works and the discussion of d'Eon and Irving [2011]. The derivation is straightforward—we simply present the final result and the comparisons.

$$2\,C_1 \approx \begin{cases} 0.919317 - 3.4793\eta + 6.75335\eta^2 - 7.80989\eta^3 \\ \qquad +4.98554\eta^4 - 1.36881\eta^5, & \eta < 1 \\ -9.23372 + 22.2272\eta - 20.9292\eta^2 + 10.2291\eta^3 \\ \qquad -2.54396\eta^4 + 0.254913\eta^5, & \eta >= 1 \end{cases} \quad (2)$$

$$3\,C_2 \approx \begin{cases} 0.828421 - 2.62051\eta + 3.36231\eta^2 - 1.95284\eta^3 \\ \qquad +0.236494\eta^4 + 0.145787\eta^5, & \eta < 1 \\ -1641.1 + \frac{135.926}{\eta^3} - \frac{656.175}{\eta^2} + \frac{1376.53}{\eta} + 1213.67\eta \\ \quad -568.556\eta^2 + 164.798\eta^3 - 27.0181\eta^4 + 1.91826\eta^5, & \eta >= 1 \end{cases}$$

3 Model Comparisons

3.1 The various plots

The followings pages contain comparisons of four different estimations of the radially-resolved exitance from a semi-infinite half space illuminated by a monodirectional beam at normal incidence (the 2D searchlight problem). The Monte Carlo reference solution, shown as dots, uses MCML [Wang et al. 1995]. The classical dipole model [Farrell et al. 1992; Jensen et al. 2001; Jensen and Buhler 2002] is shown in red, the quantized-diffusion model presented in [D'Eon and Irving 2011] is shown in orange, and the dashed lines shown the better dipole model. The last page shows a single material simulation with the various individual improvements turned on/off so that their individual effects can be seen.

3.2 Single Scattering

The quantized-diffusion model added to a single-scattering calculation is shown is green (in this case the single-scattering result was computed using numerical integration in Mathematica). We stress again that the portion of the BSSRDF described by diffusion theory (ie. by the dipole or quantized diffusion) does *not* attempt to include single-scattering and should not. The attempt of classical diffusion theory to incorporate single scattering is the primary cause for its inaccuracy as absorption levels increase and near sources (more on this and the success of the Grosjean modification is given in [D'Eon and Irving 2011]). This is why all plots except green (which is the only one which adds single-scattering to the analytic diffusion result) differ from Monte Carlo for very small r, and also why the classical dipole, shown in red, tends to consistently perform poorly for low r. Given that the quantized diffusion result does not match the dipole result in general and also given that the quantized diffusion result when added to single-scattering does match Monte Carlo quite well, it should then be clear that adding single-scattering to the classical dipole (not shown) would not be accurate in general and would not improve its performance.

The diffuse albedo reported in each plot is the one from the Monte Carlo simulation and includes the energy of single-scattering (but not specular) (and therefore is not necessarily close to the albedo of the diffusion dipole functions themselves).

3.3 Discussion

Each page presents a single fixed absorption/scattering ratio and a range of indices of refraction. Only the ratio of absorption to scattering changes the total diffuse albedo, so it is only necessary to consider the various ratios and not an array of combinations of μ_a and μ_s'. Each result is plotted in two forms, one "Gamma" plot which is well suited for evaluating the performance of a 2D radial convolution profile in the context of image synthesis, and a log plot typical of other fields and for highlighting the performance of diffusion methods far from the source, but potentially down-playing enormous errors near the source.

The first few pages show incredibly low absorption levels. This is a regime where single-scattering is a very small part of the total energy leaving the medium and also a regime where classical

Term	Classical Dipole	Better Dipole
$D =$	$\frac{1}{3\mu_t'}$	$\frac{2\mu_a+\mu_s'}{3(\mu_a+\mu_s')^2}$
$A =$	$\frac{1+2C_1}{1-2C_1}$	$\frac{1+3C_2}{1-2C_1}$
$z_b =$	$2AD$	$2AD$
$z_r =$	$\frac{1}{\mu_t'}$	$\frac{1}{\mu_t'}$
$z_v =$	$-z_r - 2z_b$	$-z_r - 2z_b$
$d_r =$	$\sqrt{r^2+z_r^2}$	$\sqrt{r^2+z_r^2}$
$d_v =$	$\sqrt{r^2+z_v^2}$	$\sqrt{r^2+z_v^2}$
$\mu_{\text{tr}} =$	$\sqrt{\frac{\mu_a}{D}}$	$\sqrt{\frac{\mu_a}{D}}$
$C_\phi =$	0	$\frac{1}{4}(1-2C_1)$
$C_{\vec{E}} =$	1	$\frac{1}{2}(1-3C_2)$
$R(r) =$	$\frac{\alpha'}{4\pi}\left[\left(C_{\vec{E}}\frac{z_r(\mu_{\text{tr}}d_r+1)}{d_r^2}+\frac{C_\phi}{D}\right)\frac{e^{-\mu_{\text{tr}}d_r}}{d_r}-\left(C_{\vec{E}}\frac{z_v(\mu_{\text{tr}}d_v+1)}{d_v^2}+\frac{C_\phi}{D}\right)\frac{e^{-\mu_{\text{tr}}d_v}}{d_v}\right]$	$\frac{(\alpha')^2}{4\pi}\left[\left(C_{\vec{E}}\frac{z_r(\mu_{\text{tr}}d_r+1)}{d_r^2}+\frac{C_\phi}{D}\right)\frac{e^{-\mu_{\text{tr}}d_r}}{d_r}-\left(C_{\vec{E}}\frac{z_v(\mu_{\text{tr}}d_v+1)}{d_v^2}+\frac{C_\phi}{D}\right)\frac{e^{-\mu_{\text{tr}}d_v}}{d_v}\right]$

Table 2: *Dipole BSSRDF comparison*

diffusion theory is fairly accurate. Except for very near the point of illumination ($r = 0$), all the models perform quite similarly and are generally accurate. As the relative index of refraction increases, however, the consistent boundary conditions and improved exitance calculation of the better dipole are clearly more accurate. The performance of the classical dipole degrades as absorption increases. Once the absorption levels are such that the albedo is around 0.25 or less there are quite large errors near the point of illumination and the log plots begin to show the improved accuracy of the modified asymptotics of Grosjean. The better dipole stays tighter to the Monte Carlo solution throughout but still drop offs for very low r because that energy has been pushed to a depth of 1 mean free path before scattering. Single-scattering can bring back some of that lost high frequency portion of the total scattered energy, but not all of it.

3.4 Conclusion

The better dipole globally outperforms the classical dipole, as was to be expected—there is clear physical reasonsing for choosing the asymptotics, boundary conditions and exitance calculations that it uses. There is little cost in adopting the better dipole—no additional exponentials or square roots are required, and the terms that change most dramatically depend only on the index of refraction (typically constant over a surface).

The conclusions of this evaluation are, however, firmly bound to the assumption of isotropic scattering. As the phase function of the scattering process diverges away from isotropic the proper decoupling from single-scattering goes out the window, for starters. It also starts to make less and less sense to make the assumption of normal incidence and to assume that the factorization of Equation 1 is at all valid. Should any of these models fair more or less accurate in these scenarios seems of little interest as they will all fail in general. However, far from sources after many scattering events have occured the similarity relations do hold and so too do the improvements shown here (for large r), so the better dipole may find use as a component of future models or in Hybrid diffusion/Monte-Carlo methods.

References

D'EON, E., AND IRVING, G. 2011. A quantized-diffusion model for rendering translucent materials. In *ACM Transactions on Graphics (TOG)*, vol. 30, ACM, 56.

DONNER, C., AND JENSEN, H. W. 2005. Light diffusion in multi-layered translucent materials. *ACM Trans. Graphic. 24*, 3, 1032–1039.

FARRELL, T. J., PATTERSON, M. S., AND WILSON, B. 1992. A diffusion theory model of spatially resolved, steady-state diffuse reflections for the noninvasive determination of tissue optical properties *in vivo*. *Med. Phys. 19*, 4, 879–888.

GROSJEAN, C. C. 1956. On a new approximate one-velocity theory of multiple scattering in infinite homogeneous media. *Il Nuovo Cimento 4*, 3 (Sep), 583–594.

GROSJEAN, C. C. 1958. Multiple Isotropic Scattering in Convex Homogeneous Media Bounded by Vacuum. *Proceedings of the Second International Conference on the Peaceful Uses of Atomic Energy 16*, 413.

JENSEN, H. W., AND BUHLER, J. 2002. A rapid hierarchical rendering technique for translucent materials. *ACM Trans. Graphic. 21*, 576–581.

JENSEN, H. W., MARSCHNER, S. R., LEVOY, M., AND HANRAHAN, P. 2001. A practical model for subsurface light transport. In *Proceedings of ACM SIGGRAPH 2001*, 511–518.

KIENLE, A., AND PATTERSON, M. S. 1997. Improved solutions of the steady-state and the time-resolved diffusion equations for reflectance from a semi-infinite turbid medium. *J. Opt. Soc. Am. A 14*, 1, 246–254.

POMRANING, G. C., AND GANAPOL, B. D. 1995. Asymptotically consistent reflection boundary conditions for diffusion theory. *Annals of Nuclear Energy 22*, 12, 787 – 817.

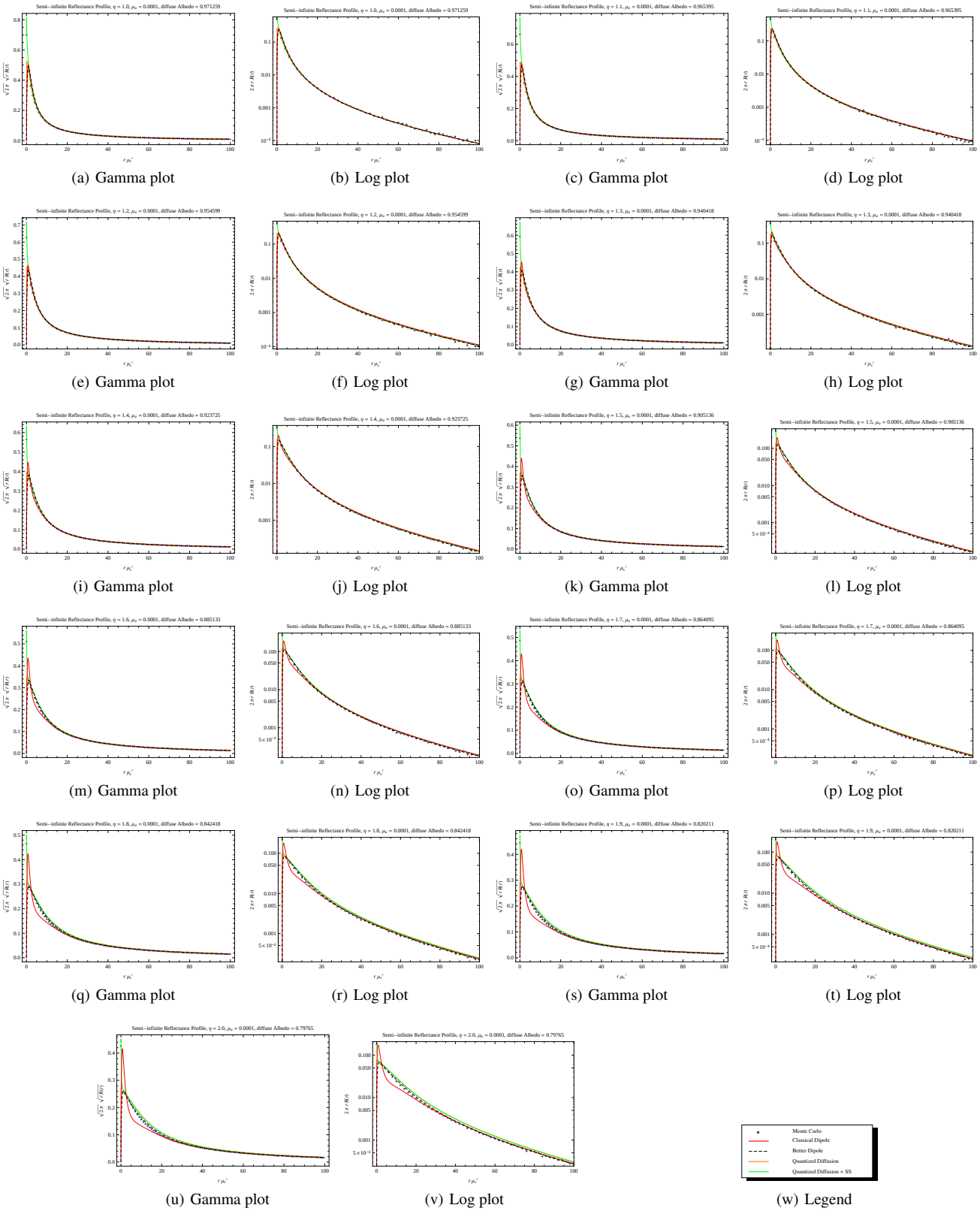

(a) Gamma plot (b) Log plot (c) Gamma plot (d) Log plot

(e) Gamma plot (f) Log plot (g) Gamma plot (h) Log plot

(i) Gamma plot (j) Log plot (k) Gamma plot (l) Log plot

(m) Gamma plot (n) Log plot (o) Gamma plot (p) Log plot

(q) Gamma plot (r) Log plot (s) Gamma plot (t) Log plot

(u) Gamma plot (v) Log plot (w) Legend

Figure 1: $\mu_a/\mu_s' == 0.0001$

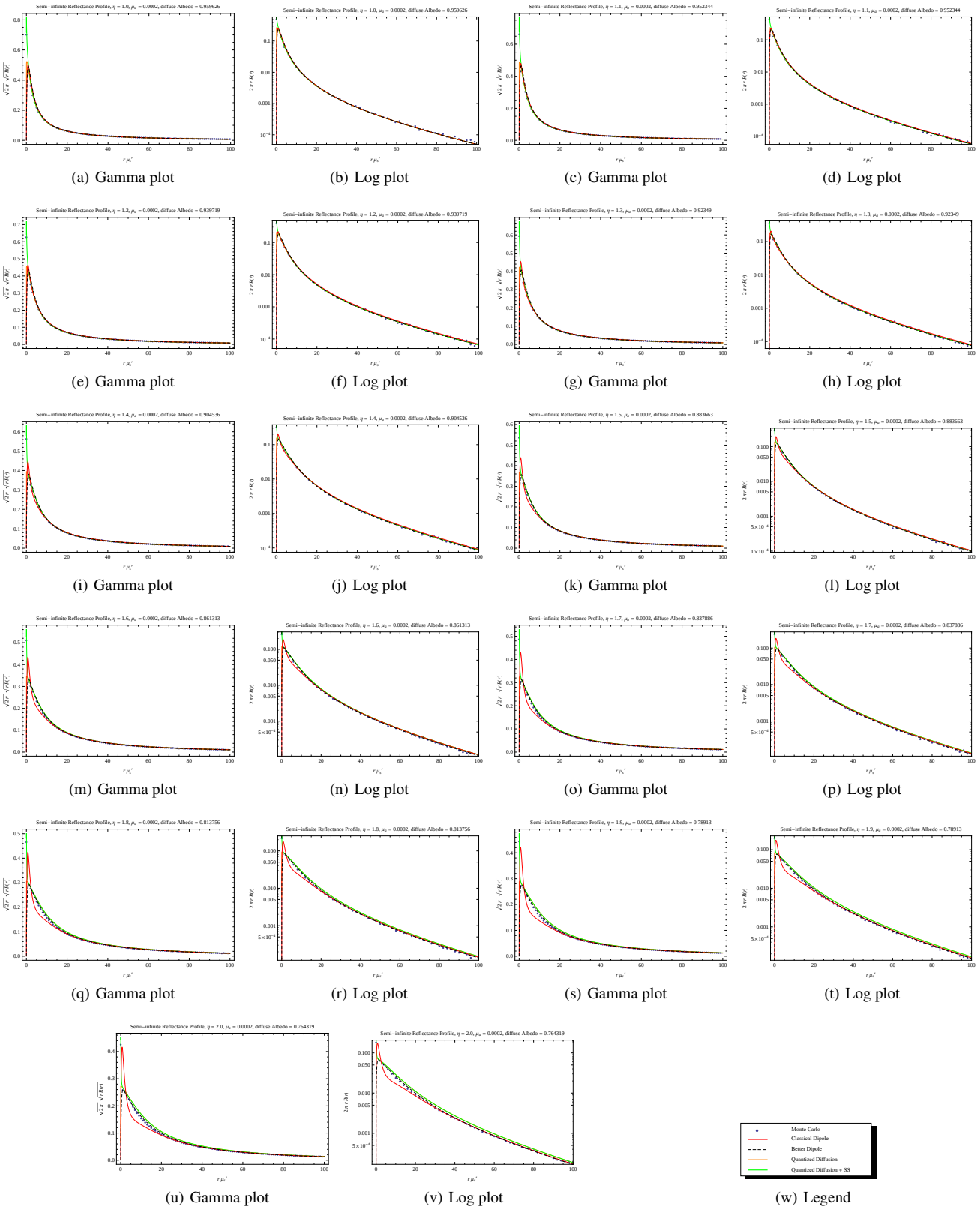

(a) Gamma plot (b) Log plot (c) Gamma plot (d) Log plot

(e) Gamma plot (f) Log plot (g) Gamma plot (h) Log plot

(i) Gamma plot (j) Log plot (k) Gamma plot (l) Log plot

(m) Gamma plot (n) Log plot (o) Gamma plot (p) Log plot

(q) Gamma plot (r) Log plot (s) Gamma plot (t) Log plot

(u) Gamma plot (v) Log plot (w) Legend

Figure 2: $\mu_a/\mu_s' == 0.0002$

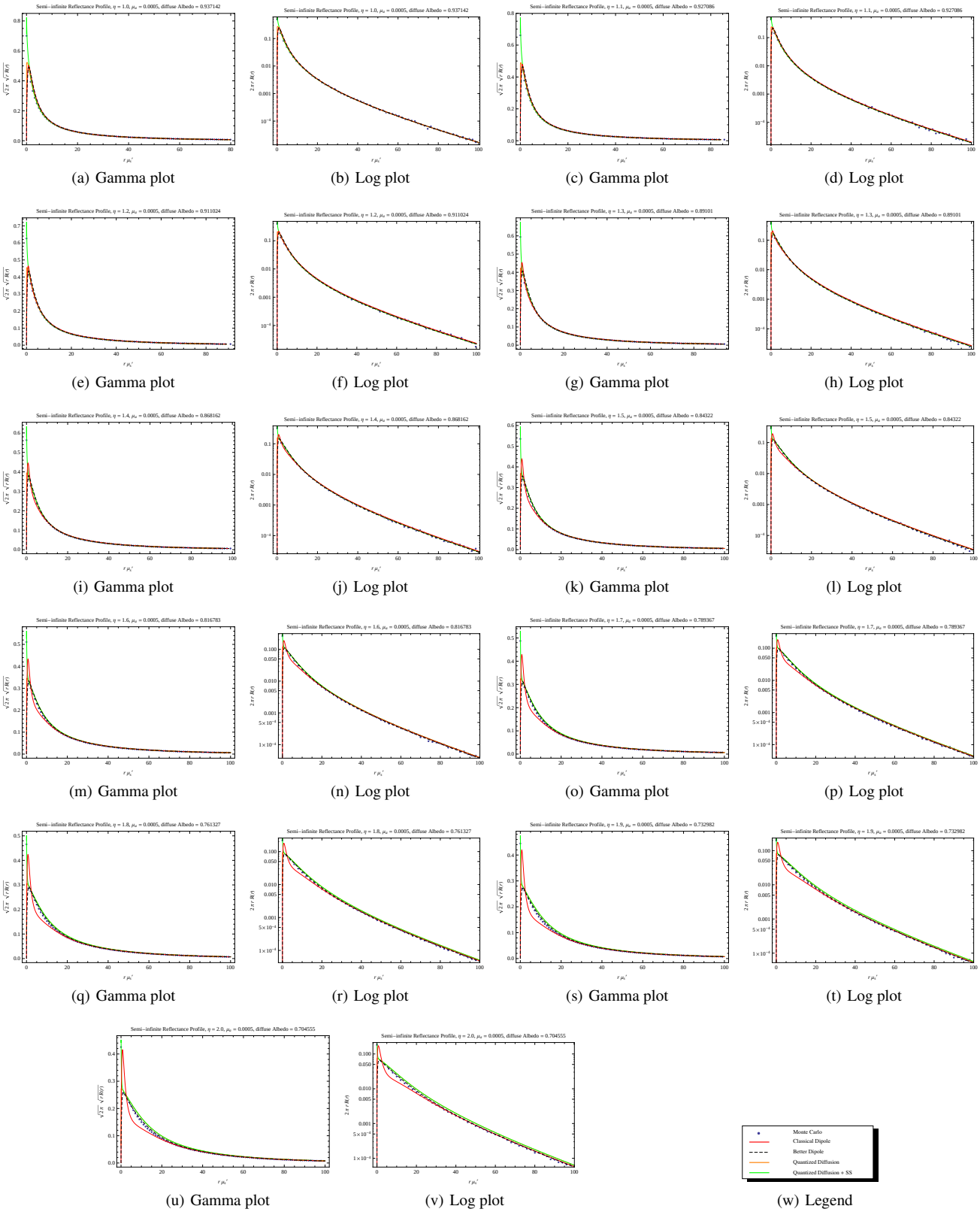

(a) Gamma plot (b) Log plot (c) Gamma plot (d) Log plot

(e) Gamma plot (f) Log plot (g) Gamma plot (h) Log plot

(i) Gamma plot (j) Log plot (k) Gamma plot (l) Log plot

(m) Gamma plot (n) Log plot (o) Gamma plot (p) Log plot

(q) Gamma plot (r) Log plot (s) Gamma plot (t) Log plot

(u) Gamma plot (v) Log plot (w) Legend

Figure 3: $\mu_a/\mu_s' == 0.0005$

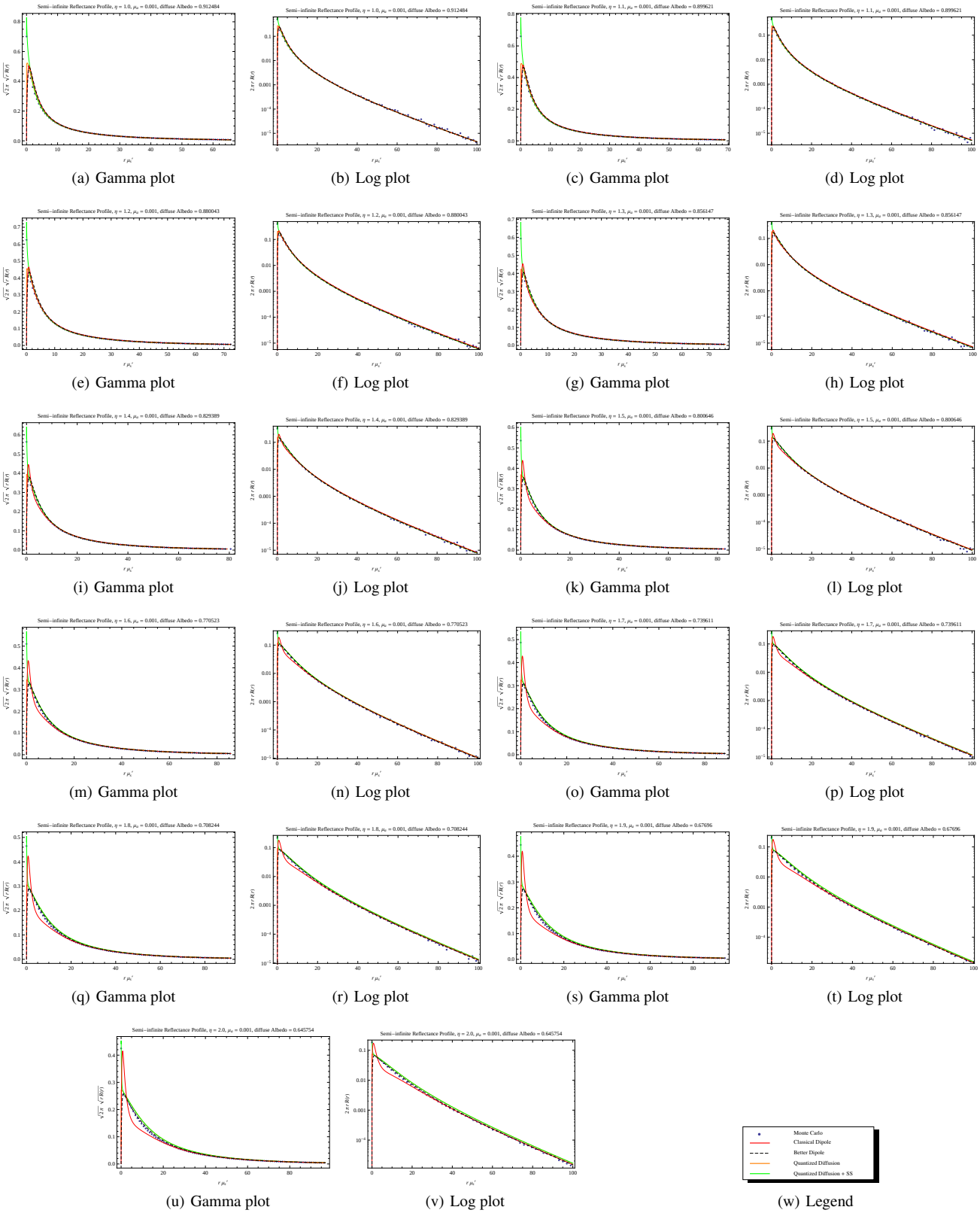

(a) Gamma plot (b) Log plot (c) Gamma plot (d) Log plot

(e) Gamma plot (f) Log plot (g) Gamma plot (h) Log plot

(i) Gamma plot (j) Log plot (k) Gamma plot (l) Log plot

(m) Gamma plot (n) Log plot (o) Gamma plot (p) Log plot

(q) Gamma plot (r) Log plot (s) Gamma plot (t) Log plot

(u) Gamma plot (v) Log plot (w) Legend

Figure 4: $\mu_a/\mu_s' == 0.001$

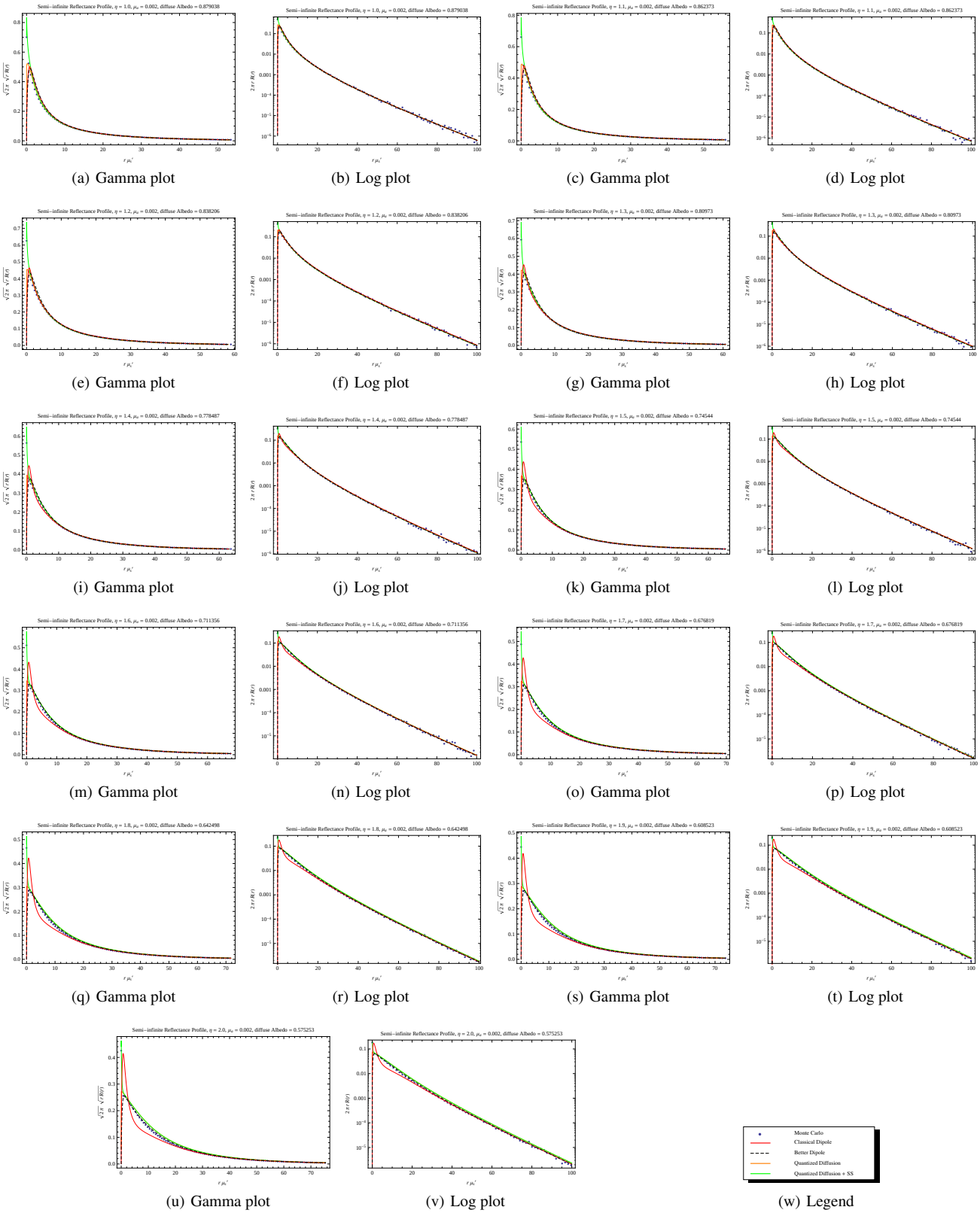

(a) Gamma plot (b) Log plot (c) Gamma plot (d) Log plot

(e) Gamma plot (f) Log plot (g) Gamma plot (h) Log plot

(i) Gamma plot (j) Log plot (k) Gamma plot (l) Log plot

(m) Gamma plot (n) Log plot (o) Gamma plot (p) Log plot

(q) Gamma plot (r) Log plot (s) Gamma plot (t) Log plot

(u) Gamma plot (v) Log plot (w) Legend

Figure 5: $\mu_a/\mu_s' == 0.002$

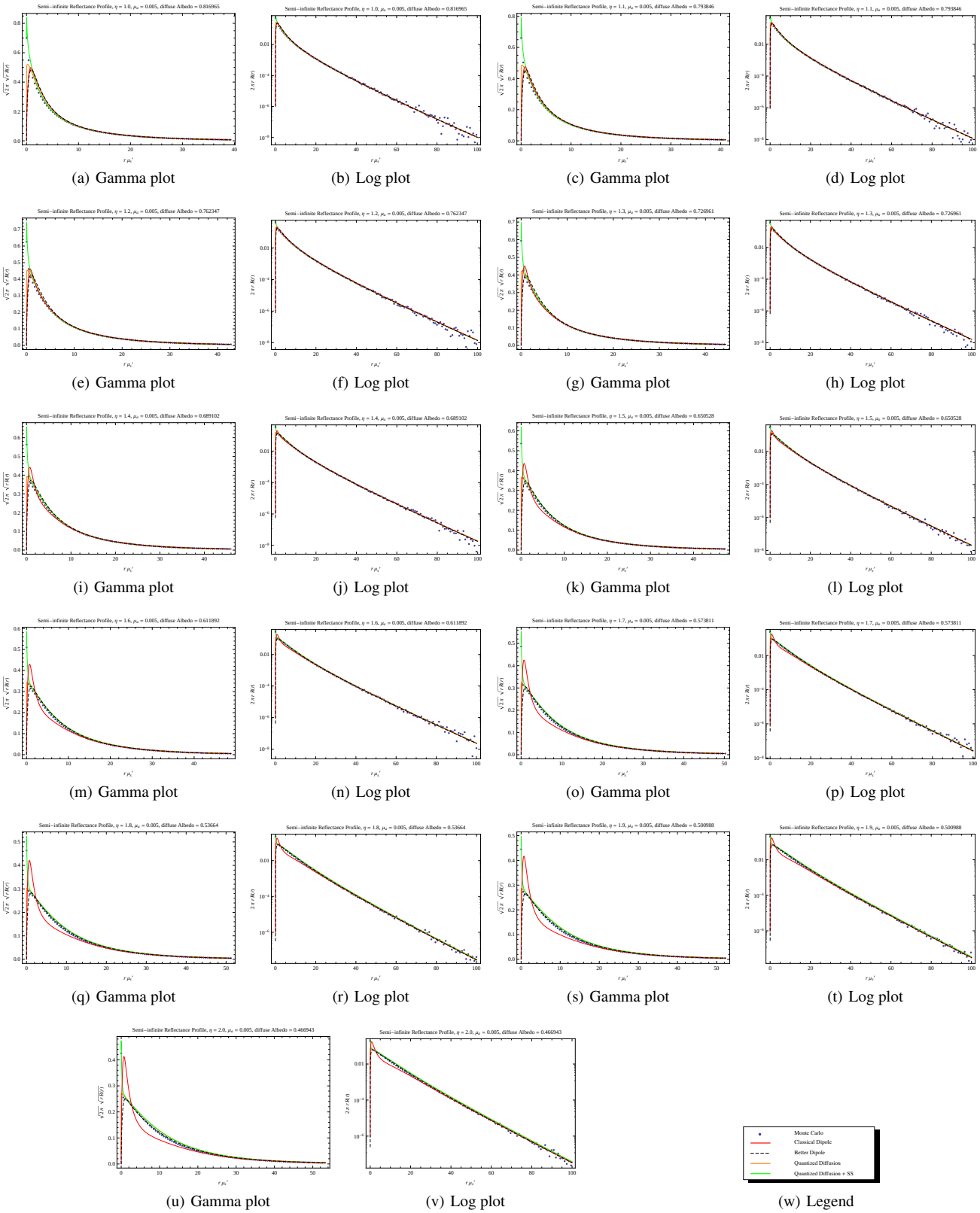

(a) Gamma plot (b) Log plot (c) Gamma plot (d) Log plot

(e) Gamma plot (f) Log plot (g) Gamma plot (h) Log plot

(i) Gamma plot (j) Log plot (k) Gamma plot (l) Log plot

(m) Gamma plot (n) Log plot (o) Gamma plot (p) Log plot

(q) Gamma plot (r) Log plot (s) Gamma plot (t) Log plot

(u) Gamma plot (v) Log plot (w) Legend

Figure 6: $\mu_a/\mu_s' == 0.005$

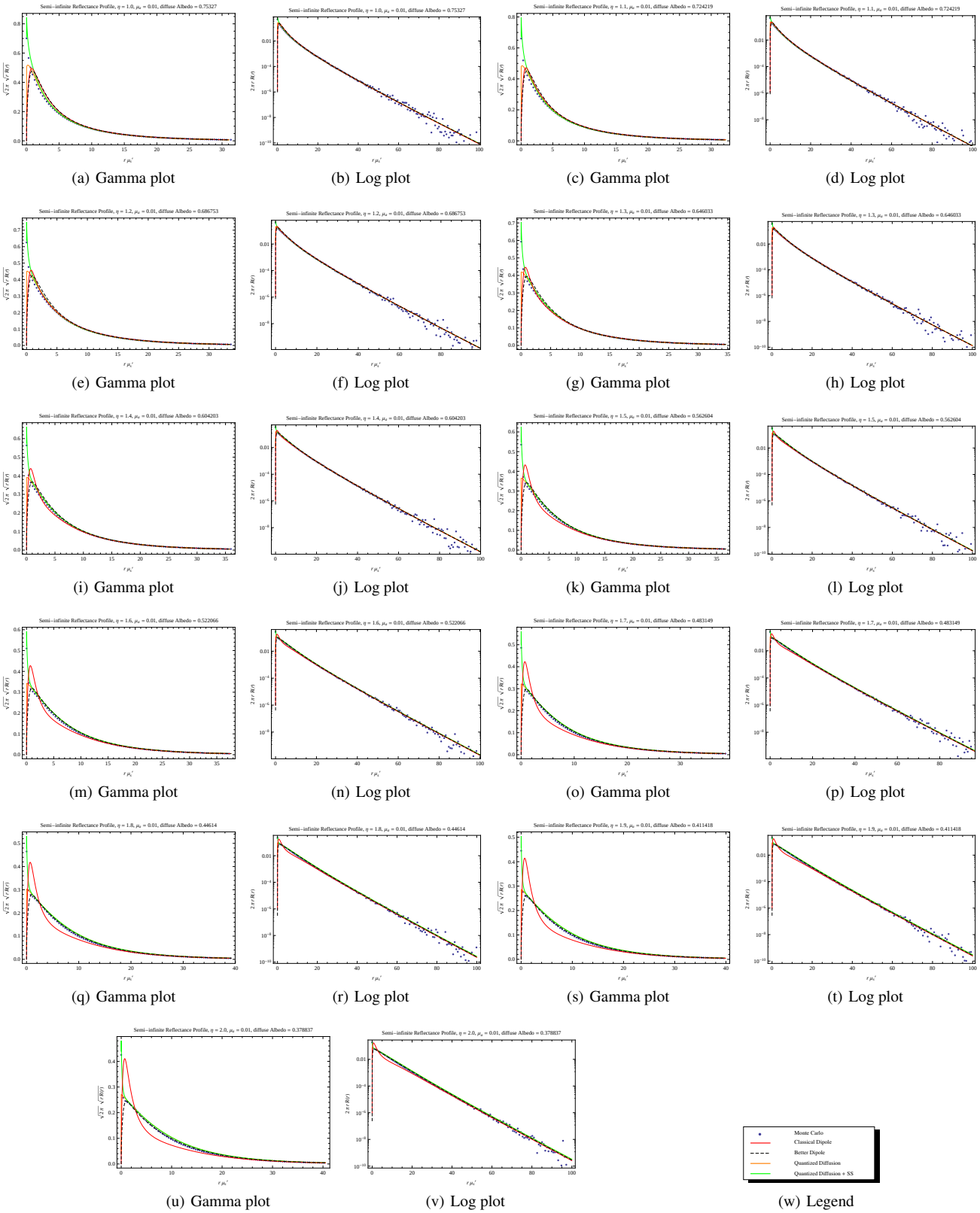

(a) Gamma plot (b) Log plot (c) Gamma plot (d) Log plot

(e) Gamma plot (f) Log plot (g) Gamma plot (h) Log plot

(i) Gamma plot (j) Log plot (k) Gamma plot (l) Log plot

(m) Gamma plot (n) Log plot (o) Gamma plot (p) Log plot

(q) Gamma plot (r) Log plot (s) Gamma plot (t) Log plot

(u) Gamma plot (v) Log plot (w) Legend

Figure 7: $\mu_a/\mu_s' == 0.01$

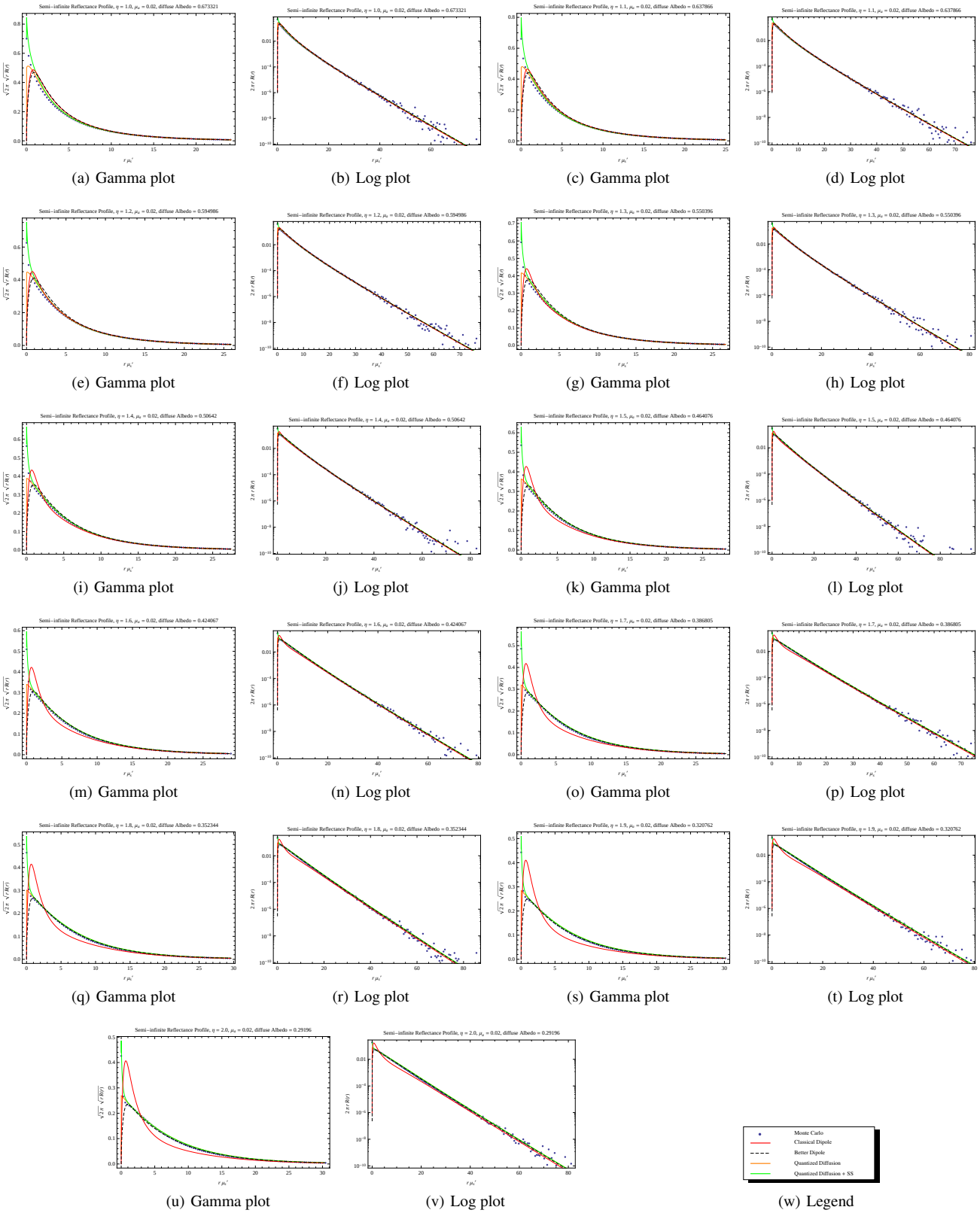

(a) Gamma plot (b) Log plot (c) Gamma plot (d) Log plot

(e) Gamma plot (f) Log plot (g) Gamma plot (h) Log plot

(i) Gamma plot (j) Log plot (k) Gamma plot (l) Log plot

(m) Gamma plot (n) Log plot (o) Gamma plot (p) Log plot

(q) Gamma plot (r) Log plot (s) Gamma plot (t) Log plot

(u) Gamma plot (v) Log plot (w) Legend

Figure 8: $\mu_a/\mu_s' == 0.02$

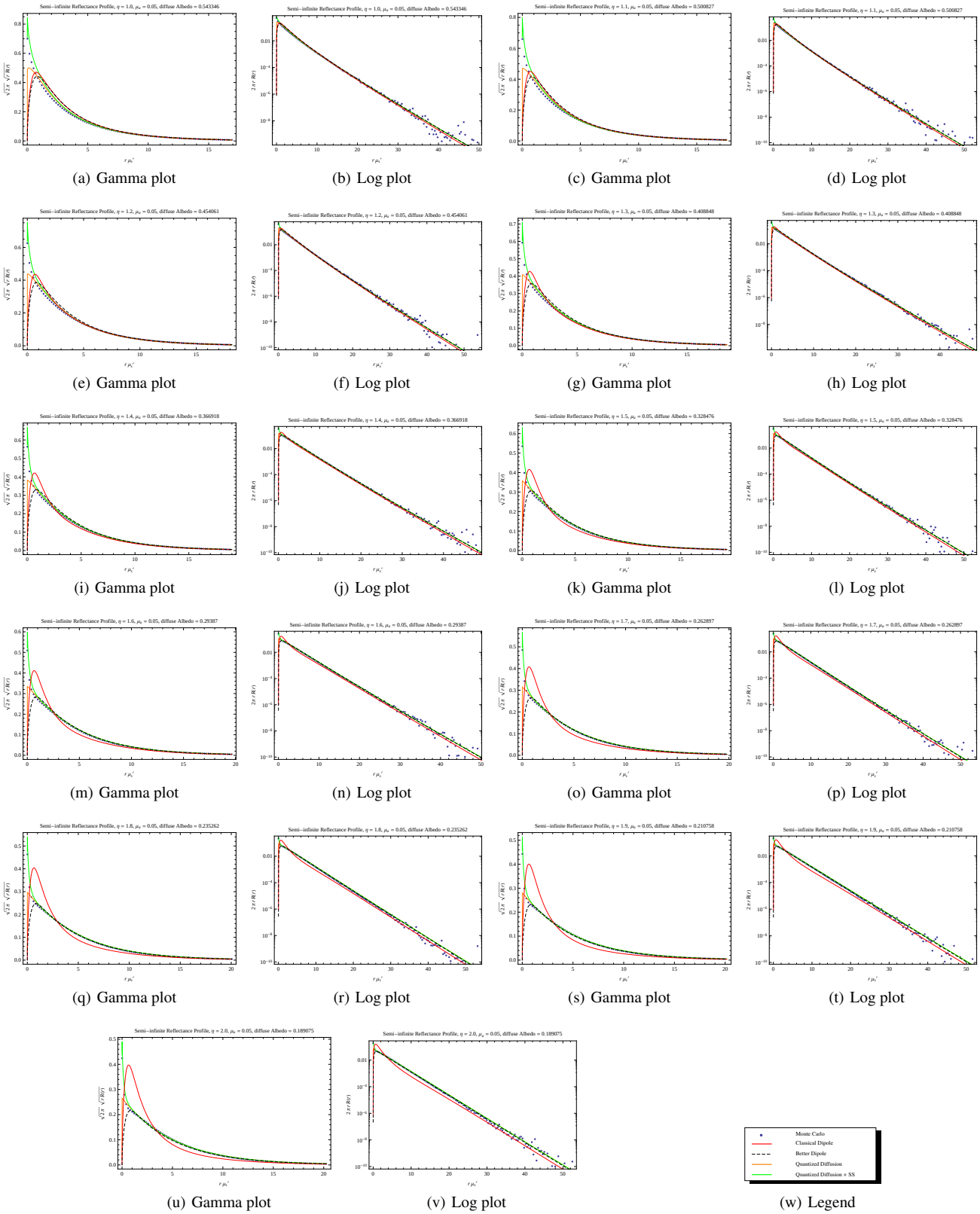

(a) Gamma plot (b) Log plot (c) Gamma plot (d) Log plot

(e) Gamma plot (f) Log plot (g) Gamma plot (h) Log plot

(i) Gamma plot (j) Log plot (k) Gamma plot (l) Log plot

(m) Gamma plot (n) Log plot (o) Gamma plot (p) Log plot

(q) Gamma plot (r) Log plot (s) Gamma plot (t) Log plot

(u) Gamma plot (v) Log plot (w) Legend

Figure 9: $\mu_a/\mu_s' == 0.05$

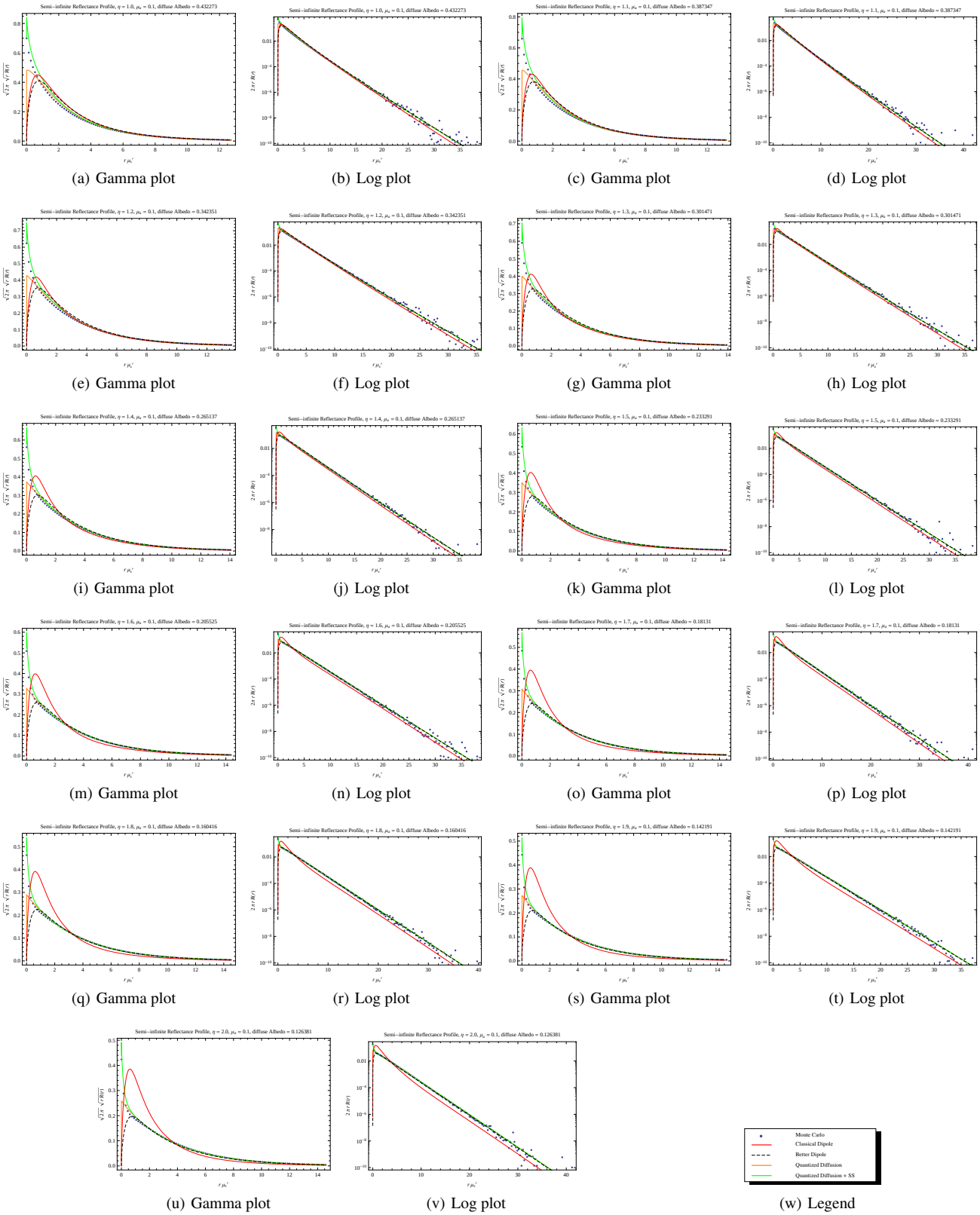

(a) Gamma plot (b) Log plot (c) Gamma plot (d) Log plot

(e) Gamma plot (f) Log plot (g) Gamma plot (h) Log plot

(i) Gamma plot (j) Log plot (k) Gamma plot (l) Log plot

(m) Gamma plot (n) Log plot (o) Gamma plot (p) Log plot

(q) Gamma plot (r) Log plot (s) Gamma plot (t) Log plot

(u) Gamma plot (v) Log plot (w) Legend

Figure 10: $\mu_a/\mu_s' == 0.1$

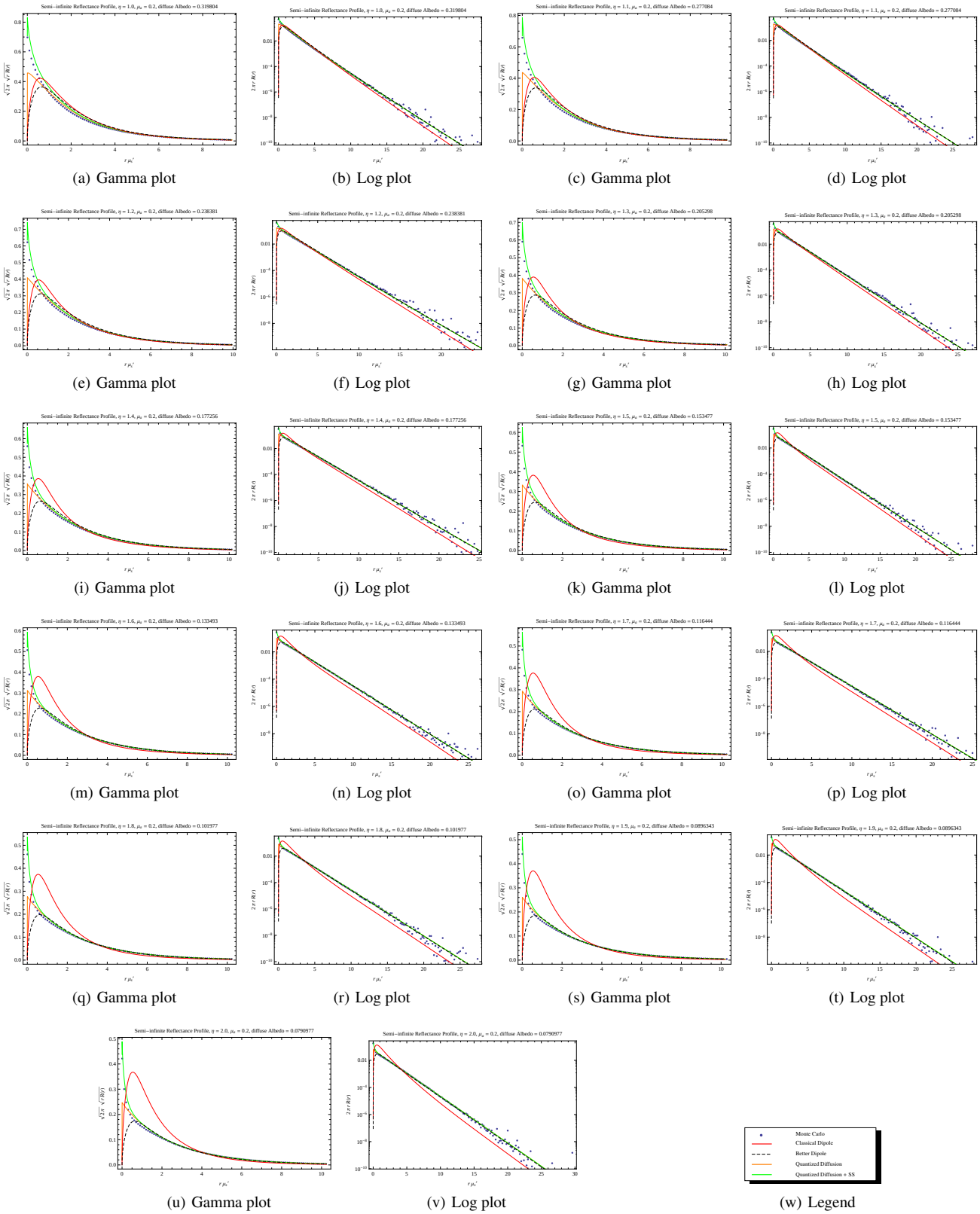

(a) Gamma plot (b) Log plot (c) Gamma plot (d) Log plot

(e) Gamma plot (f) Log plot (g) Gamma plot (h) Log plot

(i) Gamma plot (j) Log plot (k) Gamma plot (l) Log plot

(m) Gamma plot (n) Log plot (o) Gamma plot (p) Log plot

(q) Gamma plot (r) Log plot (s) Gamma plot (t) Log plot

(u) Gamma plot (v) Log plot (w) Legend

Figure 11: $\mu_a/\mu_s' == 0.2$

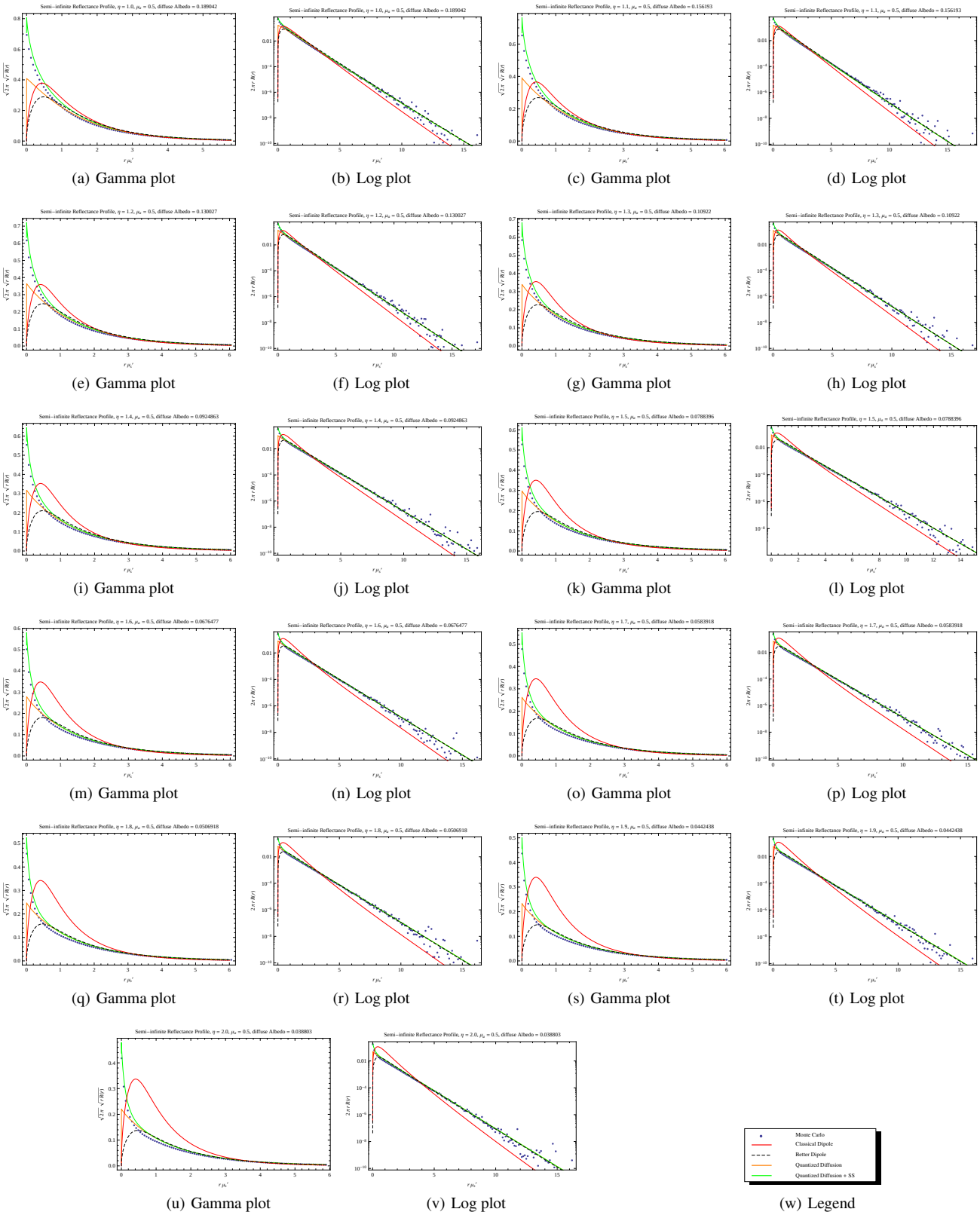

(a) Gamma plot (b) Log plot (c) Gamma plot (d) Log plot

(e) Gamma plot (f) Log plot (g) Gamma plot (h) Log plot

(i) Gamma plot (j) Log plot (k) Gamma plot (l) Log plot

(m) Gamma plot (n) Log plot (o) Gamma plot (p) Log plot

(q) Gamma plot (r) Log plot (s) Gamma plot (t) Log plot

(u) Gamma plot (v) Log plot (w) Legend

Figure 12: $\mu_a/\mu_s' == 0.5$

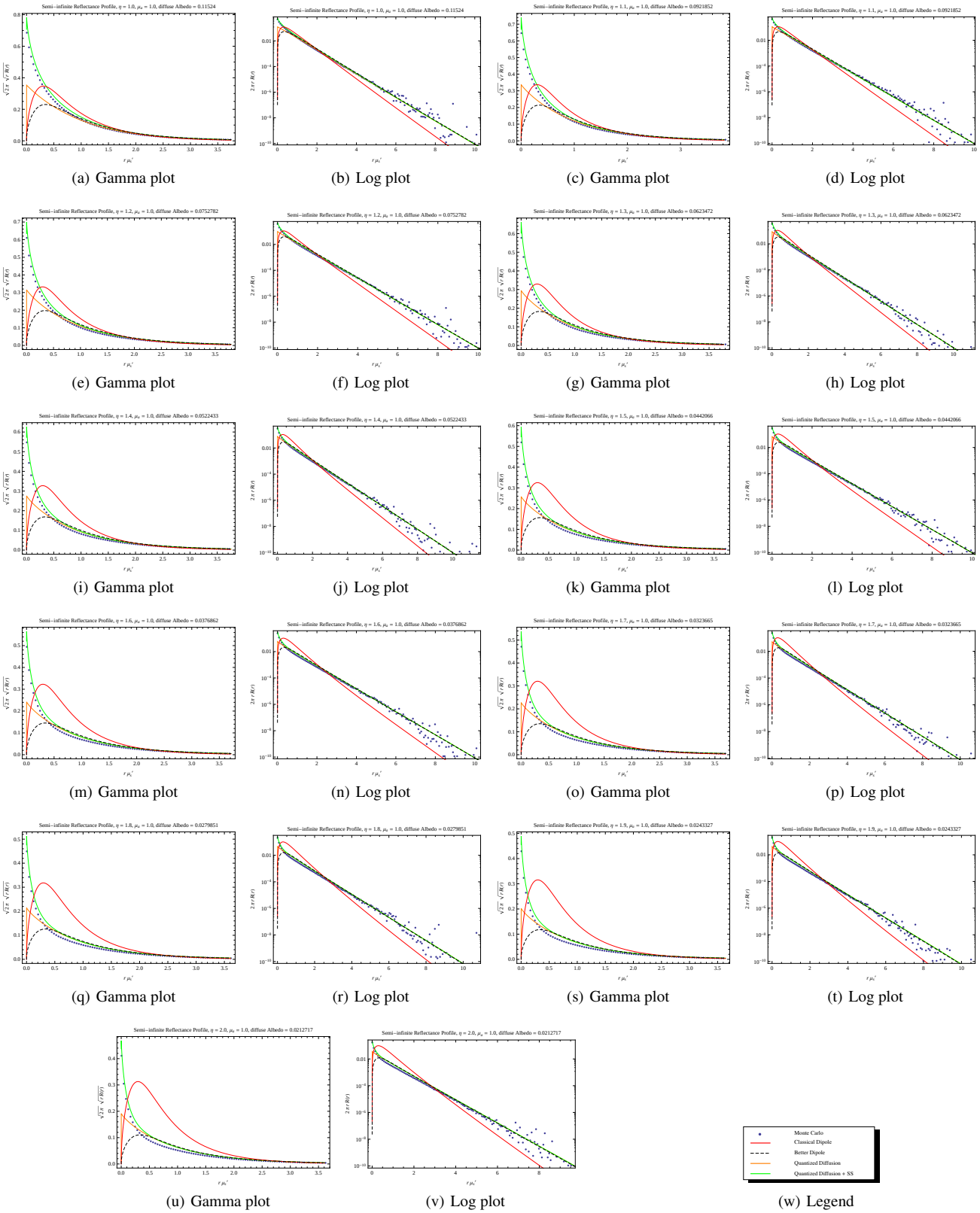

(a) Gamma plot (b) Log plot (c) Gamma plot (d) Log plot

(e) Gamma plot (f) Log plot (g) Gamma plot (h) Log plot

(i) Gamma plot (j) Log plot (k) Gamma plot (l) Log plot

(m) Gamma plot (n) Log plot (o) Gamma plot (p) Log plot

(q) Gamma plot (r) Log plot (s) Gamma plot (t) Log plot

(u) Gamma plot (v) Log plot (w) Legend

Figure 13: $\mu_a/\mu_s' == 1$

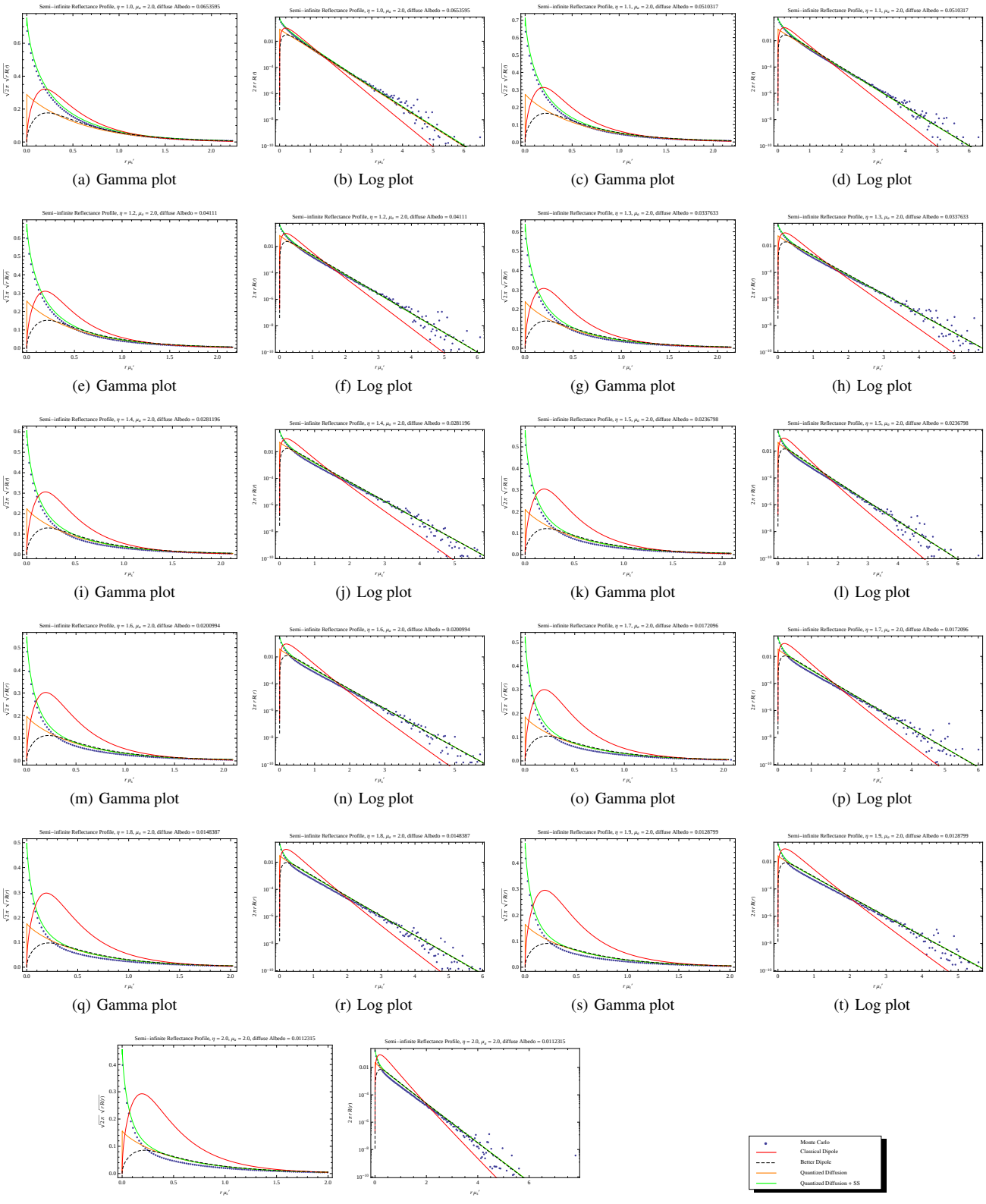

(a) Gamma plot (b) Log plot (c) Gamma plot (d) Log plot

(e) Gamma plot (f) Log plot (g) Gamma plot (h) Log plot

(i) Gamma plot (j) Log plot (k) Gamma plot (l) Log plot

(m) Gamma plot (n) Log plot (o) Gamma plot (p) Log plot

(q) Gamma plot (r) Log plot (s) Gamma plot (t) Log plot

(u) Gamma plot (v) Log plot (w) Legend

Figure 14: $\mu_a/\mu_s' == 2$

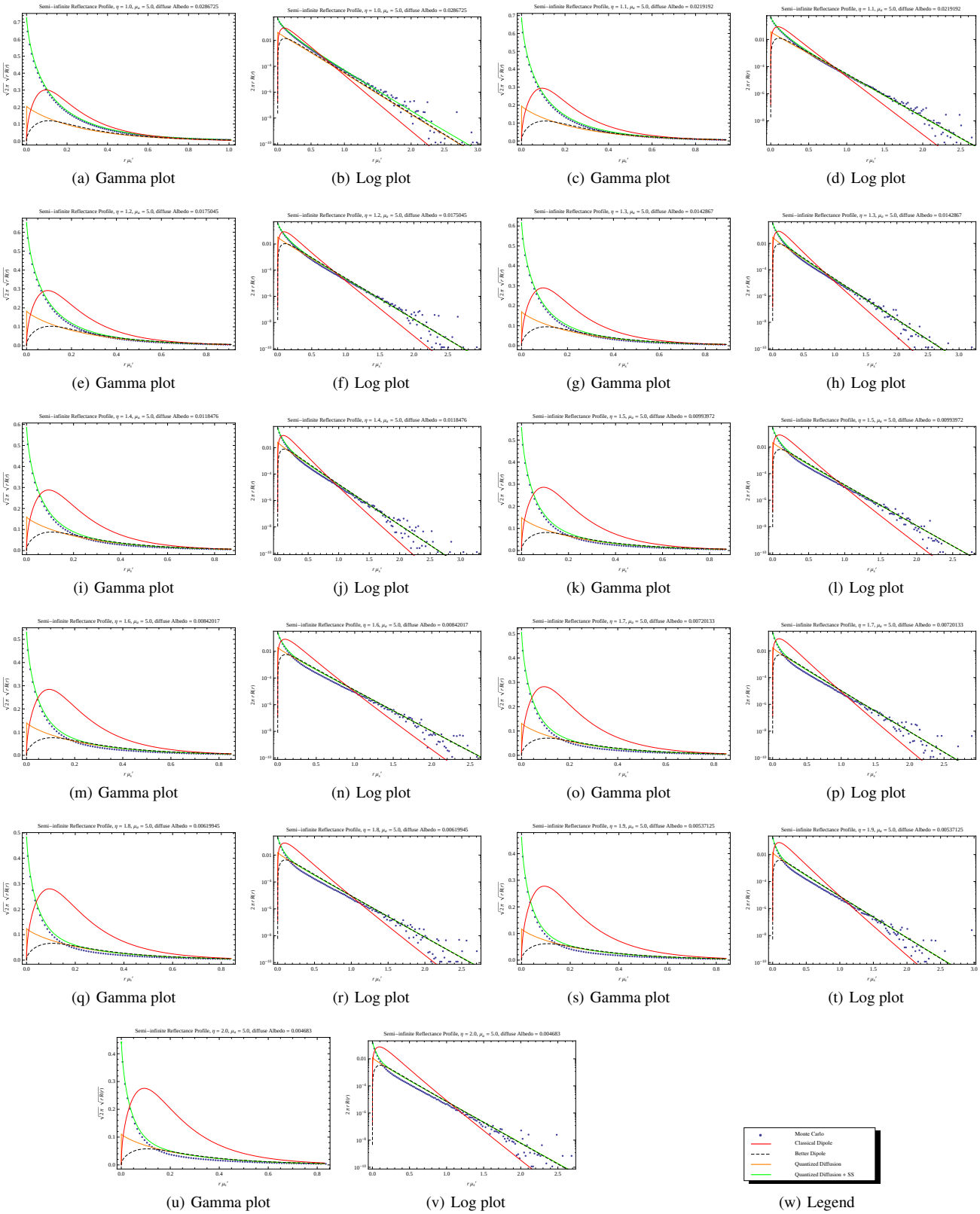

(a) Gamma plot (b) Log plot (c) Gamma plot (d) Log plot

(e) Gamma plot (f) Log plot (g) Gamma plot (h) Log plot

(i) Gamma plot (j) Log plot (k) Gamma plot (l) Log plot

(m) Gamma plot (n) Log plot (o) Gamma plot (p) Log plot

(q) Gamma plot (r) Log plot (s) Gamma plot (t) Log plot

(u) Gamma plot (v) Log plot (w) Legend

Figure 15: $\mu_a/\mu_s' == 5$

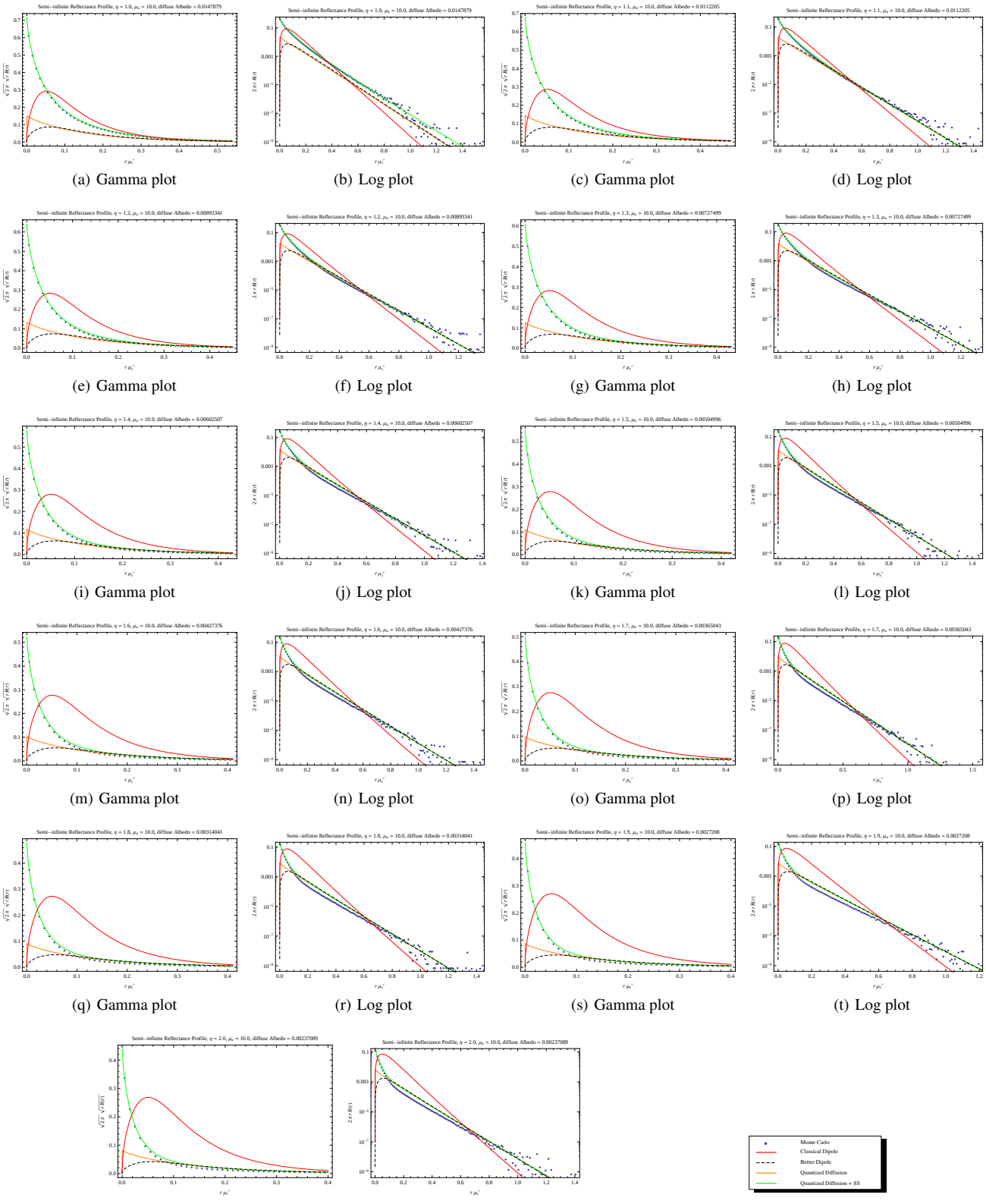

(a) Gamma plot (b) Log plot (c) Gamma plot (d) Log plot

(e) Gamma plot (f) Log plot (g) Gamma plot (h) Log plot

(i) Gamma plot (j) Log plot (k) Gamma plot (l) Log plot

(m) Gamma plot (n) Log plot (o) Gamma plot (p) Log plot

(q) Gamma plot (r) Log plot (s) Gamma plot (t) Log plot

(u) Gamma plot (v) Log plot (w) Legend

Figure 16: $\mu_a/\mu_s' == 10$

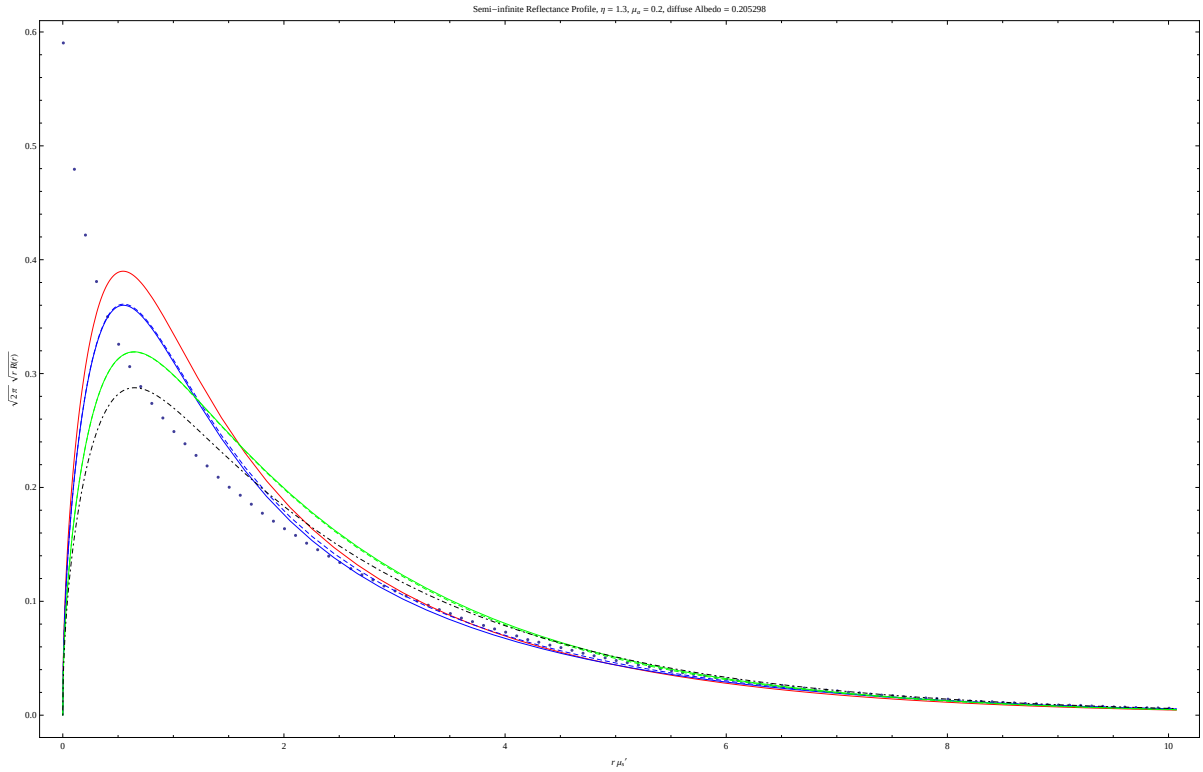

(a) Gamma plot

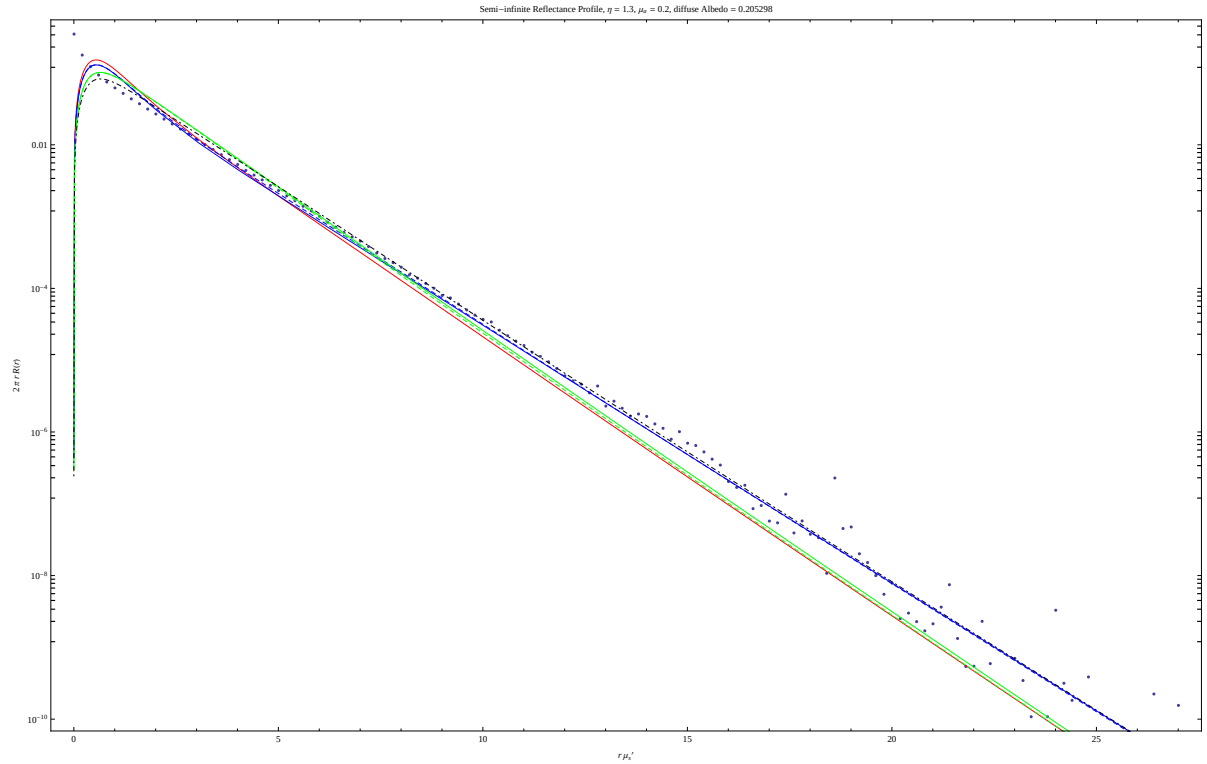

(b) Log plot

Figure 17: *Comparison with various individual modifications active. The red curve is the classical dipole. The dashed curves use the improved diffusion boundary conditions. The Blue curves use Grosjean's modified diffusion but classical exitance calculations. The Green curves use the improved exitance calculation but classic diffusion theory. The dot-dashed curved is the better dipole.*

WANG, L. V., JACQUES, S. L., AND ZHENG, L. 1995. Mcml – monte carlo modeling of light transport in multi-layered tissues. *Computer Methods in Programs and Biomedicine 47*, 8, 131–146.